PAPER

Check for updates

Introducing thermo-mechanochemistry of lignin enabled the production of high-quality low-cost carbon fiber†

Yixin Luo, Moham Ed Abdur Razzaq, Wangda Qu, Abdulrahman A. B. A. Mohammed, Alvina Aui, Hamidreza Zobeiri, Mark Mba Wright, [ID] Xinwei Wang [ID] and Xianglan Bai [ID] *

Producing green carbon fiber from lignin is not only attractive to biorefineries for valorizing lignin but also contributes to the decarbonization of multiple industries. However, the difficulty of obtaining high-quality lignin-based carbon fibers at low cost remains the bottleneck and barrier to its commercial application. Previous approaches for chemically modifying lignin or blending with co-precursors were ineffective in delivering the carbon fiber with the desired quality. We discovered that introducing thermo-mechano-chemistry of lignin to carbon fiber processing is a facile and green approach to overcome this challenge. Thermo-mechanochemistry can be introduced by properly integrating thermal heating and mechanical tension force applied to the spun fiber, which can manipulate the ordinary lignin chemistry to control the microstructure evolution from lignin. Under the influence of this newly known chemistry, lignin can transform into an oriented structure that can easily be graphitized at low temperatures. In this work, three precursors consisting of lignin or lignin blends were used to produce the carbon fibers with average tensile strength and modulus of 2.45 GPa and 236 GPa, 2.11 GPa and 215 GPa, 2.2 GPa and 225 GPa, respectively, using a surprisingly low carbonization temperature of only 700 °C. The preliminary techno-economic analysis suggests a low production cost. The discovery of the thermo-mechanochemistry of lignin will alter perceptions of lignin-based carbon fibers and provide opportunities to produce commercially viable low-cost green carbon fibers, advancing lignin valorization.

1. Introduction

Lignin is a byproduct abundantly available from paper industries and emerging biorefineries, with an estimated 225 million tons expected annually by 2030.[1] Less than 2% of the paper industry-produced lignin is utilized for chemical production, with the rest being burned as boiler fuel. Accordingly, cost-effective lignin valorization at a market-size compatible strategy remains a significant challenge.[1–3] Lignin-based carbon fiber (CF) offers a promising opportunity to valorize lignin.[4–7] CF is a lightweight material with superior mechanical properties. It is popular in applications where high mechanical properties are available at light material weights, such as aerospace, automobile, wind turbine, construction, infrastructure, and sporting goods industries.[4] For example, lightweight vehicles partly constructed with CF can improve fuel efficiency, contributing to decarbonization in the transportation sector.[8] The CF composites market size continues to increase due to the unique advantages they can offer. According to market research, the CF and CF reinforced product market is projected to grow to $31.5 billion by 2025.[9] Despite increasing demand, CF is mostly used in higher-end products due to its high costs. Over 60% of globally produced CFs are used in the aerospace and defense industries. Only 6.5% is used in the automotive industry, and 7% is used in wind turbines.[10] About 82% of global CF is produced from polyacrylonitrile (PAN), whose price accounts for 51% of CF production cost.[4–6] While commercial PAN-based CFs have tensile strength ranging from 3–7 GPa and a tensile modulus from 200 to 500 GPa, and the US Department of Energy (DOE) stated earlier that alternative precursor-based CFs with a tensile strength of 1.72 GPa and a modulus of 172 GPa, available at <$5–7 per lb could be widely used in automobile industries for the vehicle bodies and parts without compromising performance.[11] Low-cost green CFs are also attractive to other industries (*e.g.*, the construction industry, power industry, and mechanical engineering) for reducing costs and replacing non-

Department of Mechanical Engineering, Iowa State University, Ames, Iowa 50011, USA. E-mail: bxl9801@iastate.edu

† Electronic supplementary information (ESI) available. See DOI: https://doi.org/10.1039/d3gc04288j

renewable materials with renewable materials to lower carbon emissions.[4]

Lignin has been extensively studied as an alternative precursor of CF because of its low costs, abundance, fixed carbon content, and absence of toxic gas emissions during its manufacturing process. However, the major bottleneck and barrier to developing commercially relevant lignin-based CFs are their poor tensile properties, far below the DOE target. So far, various lignins with different biomass origins isolated using different extraction methods have been studied. Other than directly spinning purified lignin, blending with other polymers or additives, or pre-modifying lignin using physical, chemical, and biological methods was also investigated.[4–7,11–13] However, the resultant CFs mostly had tensile strengths below 1 GPa and tensile modulus below 100 GPa.[6] A few previous CFs with relatively higher properties are the CF with a tensile strength of 1.07 GPa and modulus of 83 GPa produced using ultra-pure, experimental-grade lignin[11] and the CF with a tensile strength of 1.39 GPa and modulus of 97 GPa obtained using solvent-fractionated and solvated kraft lignin that had ultra-high molecular weights.[14] Previous studies indicated that the difficulties in producing quality CFs are mainly attributed to the intrinsic deficiencies of lignin as a precursor of CF.[4–7] It was suggested that ideal precursors of CF must satisfy multiple requirements, such as high purity, high molecular weights, low polydispersity, and molecular orientation. Among them, the molecular linearity of a precursor is the most important factor in obtaining high-quality CFs.[4,6,11] Usually, the tensile properties of a material are strongly correlated with the molecular orientation of the precursor.[15] For example, PAN-based CFs are exceptionally strong due to the uniaxial orientation of polymer crystals along the fiber that could be graphitized into highly ordered structures. However, lignin is heterogeneous and intrinsically absent of molecular orientation.[4–6] Lignin is a polyaromatic molecule in which three primary phenylpropane monomer units, coumaryl (H type), coniferyl (G type), and sinapyl alcohols (S type), are randomly crosslinked by C–O–C (β-O-4, α-O-4, and 4-O-5) or C–C (5–5, β-5 and β-1) bonds.[16] Thus, lignin builds an amorphous three-dimensional network instead of the one-dimensional chain characteristic of most synthetic polymers. Furthermore, functional groups such as methoxyl, phenolic hydroxyl, aliphatic hydroxyl, benzyl alcohol, noncyclic benzyl ether, and carbonyl groups in lignin side chains contribute to the irregular, highly branched polymer structure. The lack of a defined molecular architecture severely limits the orientability of the drawn fibers, limiting their ability to graphitize upon carbonization.[7] In previous studies, lignin with a higher content of aryl–ether linkage was prepared,[17] or lignin was mixed with other well-defined linear long-chain polymers[18–21] to increase precursor orientability. Unfortunately, these approaches still could not yield CFs with satisfactory tensile properties. Among the approaches, blending lignin with excessively high amounts of PAN and gel-spinning the solvent-doped mixed precursors at subzero temperatures followed by subsequent processing was most efficient in improving the CF properties.[22] However, blending with PAN

increases production costs and it is questionable if such CFs are still called lignin-based CFs. In summary, while lignin-based CFs were extensively investigated, the mechanical properties of previous CFs have been insufficient for use in structural applications. In this context, we previously used lignin bio-oil consisting of phenolic monomers and oligomers to synthesize acrylate polymers using a controlled radical polymerization technique.[23,24] The lignin-derived linear thermoplastic polymer is further processed into CFs with a tensile strength of 1.7 GPa and tensile modulus of 182 GPa.[24] These values are higher than previous results, emphasizing the importance of structural linearity in CF production.

While the previous studies mainly focused on modifying precursors, an overlooked aspect is the fiber fabrication process that transforms lignin into a CF structure. The fiber fabrication process of lignin-based CF is generally similar to that of PAN-based CF; both include fiber spinning, oxidative thermal stabilization, and carbonization. During the two-step thermal treatments, precursor fibers are chemically transformed to form carbonized materials. PAN is a linear one-dimensional long-chain polymer with repeated units. Since PAN does not melt before decomposing, PAN doped in a dissolving solvent is spun into a fiber form. The fiber is then rinsed in a water bath to remove the dissolving solvent. PAN has no fixed carbons and thus cannot be directly carbonized. Thus, spun fibers had to be first stabilized oxidatively to convert PAN into a new structure that can be carbonized. In the stabilization, PAN-spun fiber is heated in air or an oxidizing environment between 200–300 °C. When oxygen atoms enter its structure, the linear polymer chains of PAN are reorganized and cross-linked to form a nitrogen-containing cyclized ladder structure.[4,25] Tension was also applied to reduce entangled polymer chains while oxidative transformation occurs. After stabilization, the fiber containing the oriented supramolecular structure is carbonized under the inert environment with temperatures above 1000 °C up to 1600 °C.[25] During carbonization, the cyclized structure undergoes dehydrogenation and condensation to form turbostratic carbons oriented in the fiber direction. The turbostratic carbon structure, where many tetrahedral carbons crosslink the graphite-type carbon layers, is responsible for the high tensile strength of PAN-based CFs.[25]

The transformation of PAN during CF production was extensively studied and well understood.[4] In comparison, much less is known about lignin transformation during its fiber fabrication. Lignin has completely different chemical structures and rheological properties than PAN. While it varies by individual lignin, lignin usually has much lower glass transition temperatures (T_g) than PAN. Thus, lignin with a sufficiently low T_g can be melt-spun at much lower costs than the solvent-based spinning of PAN fibers (*e.g.*, about 1/10th of the cost).[5] Unlike PAN, lignin contains oxygenated functional groups and thus can be carbonized. However, the lignin-spun fibers soften at elevated temperatures, causing the fiber to fuse or melt.[11] Therefore, the fusible spun fibers must be converted to non-fusible fibers by stabilization. During stabilization,

lignin-spun fibers were heated in the air at temperatures below 300 °C, where oxygen promotes crosslinking of lignin and thus increases the fiber T_g.[11,26] Other than the fiber fusing, the as-spun fiber of lignin is also much weaker and significantly more brittle than the strong PAN-spun fiber. The weak spun fibers of lignin are attributed to low molecular weights, high dispersity, and lack of molecular orientation in lignin.[6] Since as-spun fibers can break or melt, stabilization was usually performed without interruption by external mechanical force. Occasionally, minimal tension force was applied while the fibers softened to reduce fiber diameters.[19,27] During the subsequent carbonization at 1000 °C or above, the stabilized fibers were further crosslinked and carbonized to remove non-carbon elements.[6] Lignin-based CFs produced using the above method have amorphous carbon structures and randomly scattered nanocrystallites[28] compared to the highly oriented turbostratic carbons found in PAN-based CFs, which explains the poor mechanical properties of lignin-based CFs.

As described above, the lack of repeated molecular units and orientation in lignin structures hindered the formation of graphene carbons and oriented structures desired for producing high-quality CFs. While lignin pretreatments or additives increased the production costs, such efforts were insufficient to overcome the tensile property issues of the CF. Lignin undergoes extensive chemical transformation and microstructural changes during the thermal treatments for producing CF. On the other hand, this also suggests that the fiber fabrication process can strongly affect the chemical reactions of lignin and microstructural evolution. However, this potential opportunity for altering lignin has been largely overlooked. Although chemical structures of raw lignins[29] or oxidized lignin[25] were analyzed in previous studies, such studies do not inform the chemical reactions nor the microstructural change dependent on the fiber processing conditions employed during actual CF production. In this work, we report a discovery of the thermo-mechanochemistry of lignin, which challenged the conventional understanding of lignin-based CF. Our findings show that a proper combination of thermal heating and mechanical tension force applied to lignin can introduce novel thermo-mechanochemistry, presenting us with an opportunity to manipulate the ordinary chemical reactions of lignin and control the microstructure evolution. Based on this approach, lignin can transform into high-quality CFs with graphitized structures and orientations without chemical treatments or additives but by applying heat and mechanical force. In the following, we will demonstrate CFs with unprecedented tensile properties produced solely from lignin and unexpectedly low carbonization temperatures for proof-of-concept. We will then track the changes in chemical and material structures of lignin at the different stages under different thermo-mechanical conditions to confirm the presence of thermo-mechanochemistry and elucidate its mechanisms for altering chemical reactions and controlling microstructural formation. Finally, we will present a cost analysis result to show the economic feasibility of lignin-based CFs.

2. Experimental

2.1. Lignin preparation

Softwood organosolv (OL) was provided by Attis, and softwood Indulin kraft lignin (KL) was obtained from Ingevity. As-received lignins were washed in 90 °C deionized water for 4 hours using a magnetic stirring bar to remove water-soluble impurities. The washed lignin was filtered and vacuum-dried overnight at 40 °C and kept in a sealed container before use.

2.2. CF production method

Melt spinning of lignin precursors was performed using a bench-top twin-screw micro compounder (DACA Instruments, Santa Barbara, CA) with a nozzle size of 2 mm, and fibers were collected on a roller (DSM, Geleen, the Netherlands) at 100 m min⁻¹. When OL was used, the lignin powder was directly injected into the extruder for fiber spinning. OL was melt-spinnable. However, KL cannot melt-spun because it did not soften before thermally decomposing. Thus, KL was blended with OL to prepare melt-spinnable precursors. The three precursors tested are 100% OL, 90/10 (w/w) OL/KL blend, and 80/20 (w/w) OL/KL blend. The blends containing higher than 20% of KL were difficult to melt spin. For preparing blended lignin precursors, OL and KL were first mixed in the extruder to make pellets. The mixing temperature was 185 °C for the 90/10 (w/w) OL/KL blend and 195 °C for the 80/20 (w/w) blend. The rotation speed was 150 rpm for both blends. The pellets were then re-injected into the extruder for fiber spinning. The extruder temperature and rotation speed were 155 °C and 100 rpm for OL, 195 °C and 100 rpm for 90/10 OL/KL, and 205 °C and 120 rpm for 80/20 OL/KL, respectively.

Stabilization was performed using an Isotemp programable forced-draft furnace (Fisher Scientific; 12 × 6 inch dimension) using air. Before stabilization, the as-spun fiber (AF) bundle was cut into a length of 2 cm. Each end of the fiber bundle was held between two graphite strips using epoxy glue. The fibers and the graphite strip assembly were vertically hung inside the furnace. Tension was applied by attaching different amounts of weights to the bottom of the fiber assembly via a hook. The amount of tension stress applied to a single fiber was calculated by dividing the total gravity weight applied on the fibers (i.e., the sum of the mass of the fibers, the graphene strips, epoxy, hook, and the metal weights) by the cross-sectional area of the fiber bundles and the number of the fibers. The weights were adjusted multiple times during the stabilization. The cross-sectional areas of the fiber bundles were measured when the weights were adjusted to calculate the tensile stress of the fibers at the times of the adjustments. The heating and tension profiles employed during the stabilization are given in Fig. 1. In this work, the stabilized fibers (SF) produced under tension-applied conditions are indicated as "TSF". For a comparison study, 100% OL-derived AF was also freely placed on an alumina boat and stabilized using the same heating profile given in Fig. 1 above for TSF but without applying tension. This non-tension applied SF is indicated as "NSF".

Fig. 1 Heating profiles and tension adjustments of spun fibers during stabilization. (a) 100% OL; (b) 90/10 OL/KL; (c) 80/20 OL/KL. Orange triangles indicate when the weight loading attached to the fibers was adjusted. Weight loading remained constant until the next adjustment. The tension stress of fibers was measured only when the weight loading was adjusted. Due to decreasing fiber diameters during stabilization, tension stress per fiber is expected to increase even with the same weight loading.

Carbonization of TSF and NSF was conducted in a tubular furnace (Lindberg Blue M, Thermo Scientific) purged by nitrogen gas. Before carbonization, the TSF bundle was placed onto a graphite sheet, and the ends of the fiber were fixed using a high-temperature glue (Ceramabond 503) to prevent fiber shrinkage. The fibers were carbonized from room temperature to 500 °C at 7 °C min^{-1}, held at 500 °C for 5 min, from 500 °C to final temperatures at 2 °C min^{-1}, and then kept for an hour. The final temperature was between 500 and 1000 °C for OL-based fibers, 700 and 800 °C for 90/10 OL/KL-based fibers, and 700 °C for 80/20 OL/KL lignin. The resulting CF prepared in the presence of tension during both stabilization and carbonization is indicated as "TCF". For a comparison study, 100% OL-based NSF or TSF were also freely placed on an alumina boat for carbonization. The fibers were carbonized using the same heating profile used to produce TCF. The resultant CFs are indicated as "NCF" (*i.e.*, the CF based on NSF) and "PCF" (the CF based on TSF), respectively. "PCF" indicates a partially-tension applied CF because tension was applied during stabilization but not carbonization. The carbonization temperatures were also included in fiber abbreviations. For example, TCFs obtained using the carbonization temperatures of 700, 800, 900, and 1000 °C are indicated as TCF700, TCF800, TCF900, and TCF1000, respectively. The fiber abbreviations and the

corresponding processing conditions of the fibers are summarized in Fig. 2.

2.3. Characterization methods

Gel Permeation Chromatography (GPC) analysis was conducted to determine the molecular weight distribution of lignin. A Dionex Ultimate 3000 series high-performance liquid chromatograph (HPLC) was equipped with a Shodex Refractive Index (RI) and Diode Array Detectors (DAD). Two Agilent PLgel 3 μm 100A0 300 × 7.5 mm (p/n PL1110–6320) columns were connected in series and maintained at 25 °C. An ultraviolet wavelength of 254 nm was used to detect the peaks. A GPC column was calibrated with six monodisperse polystyrene standards ranging from 162 to 45 120 g mol^{-1}. Tetrahydrofuran (THF), with a flow rate of 1 mL min^{-1}, was used as solvent and eluent in the column. The lignin samples were acetylated before the GPC analysis to increase their solubility using a previous method.[30] Briefly, 100 mg of lignin was placed in a glass vial, and 3 mL of pyridine and 3 mL of acetic anhydride were added. The mixture was heated in an oil bath at 80 °C for three hours under continuous agitation. After the reaction, the solution was added to 500 mL of deionized water to precipitate the acetylated lignin. Precipitated lignin was filtered and
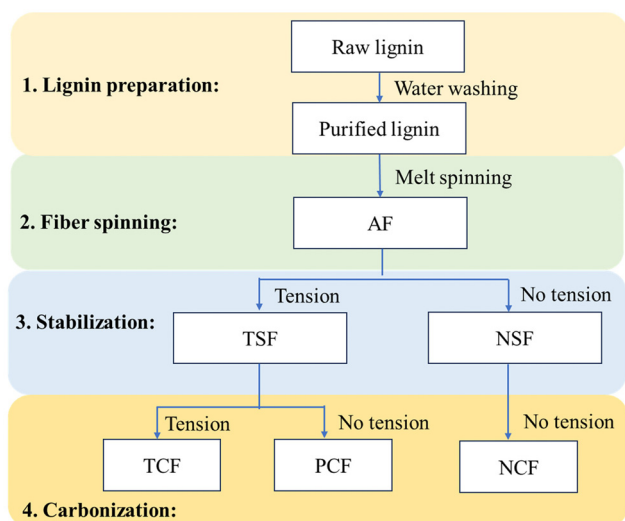
Fig. 2 Preparations of stabilized fibers and carbon fibers under different tension conditions.

washed with deionized water three times to remove the unreacted pyridine and acetic anhydride.

Proximate analysis of lignin was performed using a thermal gravimetric analyzer (TGA/DSC 1 STARe system, Mettler Toledo). About 20 mg of vacuum-dried lignin was pyrolyzed at 10 °C min^{-1} to 900 °C using nitrogen with a flow rate of 100 mL min^{-1}. After staying at 900 °C for 30 min, the air was introduced for combustion.

The glass transition temperature of lignin was determined using a DSC (Q2000, TA instruments). The sample was first rapidly heated to 200 °C and then cooled to 25 °C to eliminate thermal history. The sample was reheated to 200 °C at a heating rate of 10 °C min^{-1} to determine T_g.

Tensile properties of fibers were measured using a Discovery hybrid rheometer (DHR-2, TA Instruments) with dynamic mechanical analysis clamps by following an ASTM standard (ASTM C1557-03) based on single filament testing protocol. Data was acquired with a 0.001 s interval during the test. The fiber diameter was determined using a calibrated Leica LED inverted laboratory microscope with a 20× magnification lens with a resolution of 1 pixel. Each fiber diameter was the average of the measurements at five different locations along the fiber axial direction. The results of an average of 20 fibers were reported with a 95% confidence interval.

Scanning Electron Microscopy (SEM) analysis of CF was performed using FEI Inspect F50 Scanning Electron Microscope.

Transmission Electron Microscopy (TEM) analysis of CF was performed using a JEOL 2100 scanning TEM (Japan Electron Optics Laboratories) with a Gatan OneView 4K camera (Gatan, Inc.) and an operating voltage of 200 kV. ImageJ was used to determine crystallite size.

For preparing samples for heteronuclear-single-quantum-coherence nuclear magnetic resonance (HSQC-NMR) analysis, 100 mg of lignin or lignin-based fibers were dissolved in 1 mL of 4 : 1 (v/v) mixture of dimethyl sulfoxide (DMSO)-d6 and pyri-

dine-d5 and sonicated for 2 hours. HSQC spectroscopies were obtained on a Bruker Biospin Advance 600 MHz spectrometer incorporated with a 5 mm cryogenically cooled z-gradient probe using the Bruker pulse sequence "hsqcetg-psisp.2". The data processing was carried out using MestReNova v12.0.1 software.

Fourier Transform Infrared (FTIR) analysis was conducted using a Thermo Scientific Nicolet iS10 (Thermo Fisher Scientific Inc., Waltham, MA) with a Smart iTR accessory. The wave numbers of the FTIR analysis ranged from 750 to 4000 cm^{-1}. Each sample was scanned 32 times at a resolution of 4 cm^{-1} and an interval of 1 cm^{-1}.

Fast pyrolysis was performed using a Frontier micropyrolyzer system with an auto-shot sampler (Rx-3050 TR, Frontier Laboratories, Japan) and a single-stage furnace oven. Before pyrolysis, fibers were kept in a sealed container. During pyrolysis, approximately 0.5 mg of the sample in a deactivated stainless cup was dropped into a furnace preheated to 550 °C. Pyrolysis vapor products were directly swept into an online GC/MS. Helium was used as both the pyrolysis and carrier gas. An Agilent 7890B GC equipped with Agilent 5977A mass-selective detector (MSD), flame ionization detector (FID), and thermal conductivity analyzer (TCD) was used. The capillary column used in the GC was a ZB-1701 (60 m × 250 mm × 0.25 mm). The injection temperature at the GC was 250 °C. The oven temperature was kept at 40 °C for 3 min and then ramped to 280 °C at 3 °C min^{-1}. Finally, the oven was held at 280 °C for another 4 minutes. The GC inlet temperature was maintained at 280 °C. The helium gas flow rate was 1 mL min^{-1}, and the split ratio at the GC inlet was 20 to 1.

The elemental composition of fibers was determined using an elemental analyzer (Vario Micro Cube, Elementar, Germany). Carbon, hydrogen, nitrogen, and sulfur contents were measured, and oxygen content was determined by mass difference. The ash content of lignin was subtracted before calculating the elemental compositions.

Raman analysis of fibers was conducted using a confocal Raman system (Voyage, B&W Tek, Inc., Olympus BX51). A 532 nm Raman laser of 16 mW was focused on the fiber with a 503 lens. The measurement was conducted in two different views of the fibers. A 20 s integration time was used to obtain the spectrum, and Origin software was used to analyze the acquired Raman spectra with Gaussian curve fitting.

The crystallographic analysis of CF was conducted using an XRD (Siemens D500 diffractometer) using copper Kα radiation (λ = 1.5432 Å) with an accelerating voltage of 45 kV and current of 30 mA within the range of 2θ from 10° to 70° and a dwell time of 2 s. The fiber bundles were used, and equatorial scans were performed perpendicularly and parallel to the fiber axis.

A Xenocs Xuess 2.0 system with Cu (1.5406 Å) radiation was used to collect XPS data of CF. In the XPS spectra, C1 spectra were deconvoluted into four Gaussian peaks: –C–C–, –C–H– at 284.8 eV, –C–O– at 286.3 eV, C=O at 288.0 eV, and –O–C=O at 289.1 eV.

A Xenocs Xuess 2.0 system with Cu (1.5406 Å) radiation was used to collect Small-angle X-ray Scattering (SAXS) data.

2.4. Techno-economic analysis (TEA) modeling

The TEA was based on the study by Ellringman *et al.*[12] and validated based on the U.S. DOE 2021 Carbon Fiber report.[31] The base case facility produces 10 000 metric tonnes (MT) of CF per year from lignin using a solvent-free melt-spinning process.

Annualized capital costs for the facility were estimated using the formula:

$$\text{Capital} = \text{DF} \times \text{investment} \times \text{area}$$

where DF is the capital discount factor given a project lifetime n (20 years) with an interest rate i (10%), and it is defined as:

$$\text{DF} = \frac{1}{(1 + i)^n}$$

The investment factor is the cost per m² of the facility, which is $1386 per m² based on ref. 12. The area was calculated from the number of manufacturing lines required. A typical manufacturing line can process 1500 metric tonnes of CF per year, and each manufacturing line occupies 8650 m². The manufacturing line cost was scaled up from 1.5 to 10 hours of stabilization time using a 0.7 economies-of-scale factor. Other capital-related costs include maintenance, insurance, and property tax, calculated as 3%, 0.5%, and 1% of the annual capital cost. CF capital cost can vary significantly due to several development factors, such as equipment type, stabilization time, and facility capacity. A DOE facility survey found that capital costs for commercial facilities varied between $110 000 and $400 000 when scaled to a common capacity of 10 000 MT of CF per year.

Operating costs include material and utility costs. The main material is lignin. Lignin is available from different commercial sources, including pulp and paper mills and lignocellulosic biorefineries. Many factors, including the quality and condition of the lignin, and alternative markets, can influence the price of lignin. According to the DOE national laboratories, lignin prices range between $44 and $176 per MT. For this solvent-free process, the cost of chemicals is assumed to be negligible. Utility costs were estimated at 28.69 kW h kg⁻¹ of CF with an electricity price of 0.0692. The electricity consumption was adjusted based on the CF conversion efficiency with a baseline of 0.476 corresponding to PAN to CF.

3. Results and discussion

3.1. TCF production using a thermo-mechanically controlled fabrication method

The mass recovery after water-washing was 95% for OL and 98% for KL. The characterizations of the purified lignins are given in Table S1 of the ESI.† The T_g of the lignin and lignin blends were 74 °C, 99 °C, and 106 °C for 100% OL, 90/10 (w/w) OL/KL blend, and 80/20 (w/w) OL/KL blend, increased with increased SKL content in the blends.

Heating rates and tension applied to AF were controlled simultaneously to produce TSF. For all AFs, their viscosity decreased rapidly once the softening points of lignin were reached. Therefore, lower heating rates were used near their softening temperatures to prevent fiber fusing. Applying tension to the softened fiber at this stage can significantly reduce fiber diameters. However, AFs at the initial stage of the stabilization were very weak and could easily break if the tension force exceeded the limit the fibers could bear. The fibers became less fusible as the stabilization progressed. Thus, heating rates and tension loading were adjusted multiple times during the stabilization. Higher heating rates were used to reduce the stabilization time without causing fiber fusing. Additionally, the mechanical strength of the hardening fiber also increased as stabilization progressed. Thus, the weights attached to the fiber bundles were periodically added to ensure the fibers were stretched using as high a tension force as the fiber could bear without breaking. Increasing tension loading was also needed, otherwise, the fibers either stopped stretching too early or shrunk back if tension loading was insufficient.

The heating and tension profiles in Fig. 1 above differed for individual precursors. Higher heating rates were applied to a higher T_g precursor-based fiber containing more SKL because it was less fusible and hardened faster at lower stabilization temperatures than a lower T_g precursor-based fiber containing less or no SKL. This is because SKL has a stronger crosslinking tendency than OL. Since the fibers hardened faster for the high T_g precursor, the tension loading was increased sooner from lower stabilization temperatures to ensure the fibers were always under strong tension force and continued to stretch. It was important to tailor the tension conditions for individual precursor fibers. Different lignin precursors had different T_gs and reactivity due to their different chemical structures. Therefore, viscosity and crosslinking degree with increasing temperature varied for different lignins. These characteristics of different lignins also lead to individual precursor fibers undergoing stabilization to demonstrate different degrees of tolerance for tension stretching. To effectively stretch fibers, the fiber had to be pulled using as strong force as possible within the limit that the applied tension did not break the fiber. Since the precursor properties determine this limit, the tension profile must be tailored for individual precursors. For example, applying the tension profile suitable for an OL/KL blended precursor to 100% OL precursor can break the fibers because the OL precursor fiber was much weaker and hardened more slowly than the KL/OL blend-based fiber due to the lower reactivity of OL than KL. On the other hand, applying the tension profile suitable for 100% OL precursor fiber to the OL/KL blended precursor fiber led to a thicker fiber after stabilization because the tension force was insufficient to stretch the more rigid and faster-hardening fiber.

In this work, the fiber diameters were measured when the tension loading was adjusted. Thus, Fig. 1 above only reports the tension stresses of individual fibers at the adjustments. Due to decreasing fiber diameters during stabilization, the

tension stresses applied to the fibers are expected to increase although the tension loading on the fiber bundles stays constant until the next adjustment. Compared to the methods used in previous studies where tension was either not applied or a fixed amount of tension was applied to stretch softened fibers, the tension and heating profiles were carefully integrated into each other in our method to ensure that the heated lignin-based fiber does not fuse while it was also stretched using near the maximum tension forces that its structure can bear. At the end of stabilization, not only did the length of the fiber stretch by around 10 times (Fig. S1†), but the stabilized fibers could also tolerate sufficiently high-tension loading, strikingly different from the weak AFs.

During the subsequent carbonization process, the TSF exhibited a strong tendency to shrink in the axial direction when the carbonization temperature exceeds ~500 °C. Such a phenomenon was not seen with previously produced lignin-based CFs. The fiber shrinkage was prevented mechanically by placing the SFs on a graphite sheet base and fixing the two ends of the fiber bundles using a high-temperature adhesive. This way, external tension force created by the adhesive and graphite sheet can overcome fiber shrinkage. In previous methods, SFs were either carbonized to the final temperature of 1000 °C or above using a single heating rate or stepwise heating profiles with increasing heating rates at higher temperature regions.[6] Our method differs from the previous methods as stepwise heating with a lower heating rate at higher temperatures was employed and most fibers were carbonized at final temperatures below 1000 °C. Higher heating rates can lead to greater fiber shrinkage to the TSF stabilized under tension stretching. As shown in Fig. S2,† the OL-based TSF shrunk so severely when it was carbonized using a single heating rate of 7 °C min^{-1} to 1000 °C, so that the shrinkage even caused the graphene sheet holder to bend along the fiber direction and broke fibers. The excessive shrinkage of the fibers was avoided in this study by lowering the heating rate at higher temperatures. Further details about the preparation and fabrication of the fibers can be found in the Experimental section.

The yields of TCFs were 48–50% for lignin and blended lignins. The microscopic images of representative CFs are shown in Fig. S3.† The fibers with diameters of a few micrometers had smooth surfaces and dense cores. The tensile properties of TCFs compared to previous CFs are listed in Table 1. The average tensile strength and modulus of the 100% OL-based TCF600 produced at a carbonization temperature of 600 °C were 1.06 GPa and 84 GPa and increased significantly to 2.45 GPa and 236 GPa for TCF700 by increasing the final carbonization temperature to 700 °C. On the other hand, the average fiber diameter decreased from 6.1 μm to 3.5 μm in the corresponding fibers. Interestingly, further increasing carbonization temperatures increased fiber diameters and decreased the tensile properties. The tensile strength and modulus of TCF800, TCF900, and TCF1000 were 2.12 GPa and 189 GPa, 1.81 GPa and 178 GPa, and 1.27 GPa and 130 GPa, respectively, and the average fiber diameters were 4.3, 4.4, and

5.9 μm. The increased CF diameters were due to the increased fiber shrinkage at higher carbonization temperatures. For 90/10 OL-based TCFs, the tensile properties were 2.11 GPa and 215 GPa for the carbonization temperature of 700 °C, 2.08 GPa and 194.1 GPa for 750 °C, and 1.94 GPa and 175.8 GPa for 800 °C. respectively. The tensile properties and fiber diameters of 90/10 OL/KL blend-based TCFs had the same temperature dependencies observed with 100% OL-based TCFs. Thus, 80/20 OL/KL blend-based fiber was carbonized using the optimal temperature of 700 °C. The resultant TCF700 had tensile properties of 2.2 GPa and 225 GPa. Representative strain-stress curves of the TCF700s are shown in Fig. S4.† Compared to previous studies, this work obtained CFs with unparalleled tensile properties using unprecedently low carbonization temperatures.

3.2. Comparison of CFs produced using different processing conditions

TCFs were produced solely from lignin without chemical treatments or additives. Instead of modifying precursors, we thermo-mechanically controlled the spun fibers undergoing stabilization and carbonization. To show that the high quality of the TCFs obtained in this work is not related to the lignin sources but due to the fiber fabrication method, OL-based CFs were also fabricated using the same heating profiles but without or partial tension control as described in the method section above.

3.2.1. The dependency of CF tensile properties on fiber processing conditions. The tensile properties of OL-based CFs produced using different fabrication methods are compared in Fig. 3. Tensile properties of NCFs (*i.e.*, thermal control-only fibers) were within the range previously reported for lignin-based CFs, significantly lower than that of TCFs (*i.e.*, the thermo-mechanically controlled fibers with their tensile properties described in section 3.1 above). This result confirms that the thermo-mechanical controlling of lignin was responsible for the CF property improvement in this work. It also shows that increasing carbonization temperature from 600 to 1000 °C led to monotonic increases in tensile strength and modulus for NCFs, which was contradictory to the temperature dependence observed for TCFs. As described above, the tensile properties in the TCFs produced using either OL or OL/KL blend decreased when carbonization temperatures increased above 700 °C. It was also found that among the three CFs produced using the same carbonization temperature of 800 °C, PCF800 (*i.e.*, the CFs produced using a partial tension control, tension applied during stabilization only) had intermediate tensile properties between NCF800 and TCF800. Specifically, the tensile strength and modulus of PCF800 were 996 MPa and 76 GPa, compared to 2.12 GPa and 189 GPa for TCF800, and 549 MPa and 48 GPa for NCF800. This result clearly shows the importance of introducing thermomechanical control of spun fiber during its stabilization and carbonization.

3.2.2. TEM results of CFs dependent on processing conditions. Transmission electron microscopy (TEM) analysis was performed to visualize the nanostructures of CFs. In Fig. 4,

Table 1 Lignin-based carbon fibers produced in this work using the heating and tension profiles provided in Fig. 1 compared to literature reported carbon fibers

Precursors	Fiber spinning method	Carbonization temperature (°C)	Tensile strength (MPa)	Tensile modulus (GPa)	Fiber diameter (μm)	Ref.
Lignin or lignin blends						
Softwood organosolv lignin	Melt	600	1060	84	6.1	This work
	Melt	700	2456	236	3.5	This work
	Melt	800	2122	189	4.3	This work
	Melt	900	1809	178	4.4	This work
	Melt	1000	1272	130	5.9	This work
Softwood organosolv lignin and kraft lignin (90/10)	Melt	700	2110	215	3.3	This work
	Melt	750	2082	198	3.6	This work
	Melt	800	1941	176	3.8	This work
Softwood organosolv lignin and kraft lignin (80/20)	Melt	700	2200	225	4.1	This work
Hardwood kraft lignin	Melt	1000	605	61	46 ± 8.0	47
Softwood kraft lignin and hardwood kraft lignin (90/10)	Melt	1000	300	30	20–90	48
Alcell organosolv lignin	Melt	1000	720	45.9	8.5	49
Softwood kraft lignin	Melt	1200	465	32	39–65	50
Switchgrass organosolv lignin	Melt	1000	587	35	16.2 ± 6.0	51
Yellow poplar organosolv lignin and switchgrass organosolv lignin (85/15)	Melt	1000	747	42	15.7	52
Solvent fractionated ultra-high molecular weight softwood kraft lignin	Dry	1000	1390	98	7	14
Chemically modified lignin						
Steam exploded hardwood lignin after hydrogenation	Melt	1000	660	45	7.6 ± 2.7	53
Phenolyzed steam exploded lignin	Melt	1000	394	36	—	54
Acetylated softwood kraft lignin	Dry	1000	1040	52	6–8	27
Pyrolysis oil of hardwood lignin	Melt	1000	855	85	29–50	55
Peracylated softwood kraft lignin	Melt	1000	750	34	17	56
Acetylated corn stover organosolv lignin	Melt	1000	454	62	39.1 ± 5.4	57
Oleic acid functionalized lignin	Melt	1000	640	71	24.8 ± 4.3	58
Acrylate thermoplastic polymer synthesized using pyrolysis oil of lignin	Melt	1000	1700	182	5.1	24
Lignin and additives						
Hardwood kraft lignin and poly (ethylene oxide) (97/3)	Melt	1000	458	59	33 ± 2	59
Hardwood kraft lignin and polyethylene terephthalate (75/25)	Melt	1000	703	94	34 ± 5	47
Hardwood kraft lignin and syndiotactic polypropene (87.5/12.5)	Melt	1000	437	54	44 ± 5	47
Pyrolysis oil of lignin and 1% organoclay	Melt	1000	438	32	47 ± 1	60
Hardwood organosolv lignin and thermoplastic polyurethane (50/50)	Melt	1400	1100	80	25 ± 3	21
Hydroxyl-modified hardwood kraft lignin and thermoplastic polyurethane (50/50)	Melt	1400	800	66	30 ± 1	21
Pyrolysis oil of hardwood lignin and polyethylene terephthalate (95/5)	Melt	1000	925	98	12.6 ± 2.1	18
Kraft lignin, polyvinyl alcohol, and graphene oxide (66/29/5)	Wet	1000	763	52	—	28
Softwood kraft lignin and cellulose (70/30)	Wet	1000	1070	76	7.6 ± 0.7	61
Lignin and PAN						
Softwood kraft lignin and PAN (35/65)	Wet	1200	1680	201	16.8	62
Annual plant soda lignin and PAN (30/70)	Gel (−50 °C)	1100	1720	250	11.0 ± 1.1	63
Annual plant soda lignin, PAN, carbon nanotube (30/70/3)	Gel (−50 °C)	1100	1400	200	8.8 ± 0.3	63
Lignosulfonate and acrylonitrile co-polymer (10/90)	Wet	1400	649	—	19.2	64
Softwood kraft lignin and PAN (50/50)	Wet	1200	1200	105.7	7.0 ± 0.3	19

NCF700, NCF800, NCF900, and NCF1000 also show amorphous carbons with randomly distributed nanocrystallites. Similar amorphous structures were reported for previous lignin-based CF.[32] The branched and heterogenous molecules of lignin make it difficult to form a graphene structure. In spite of that it has been reported that lignin does not graphi-

Fig. 3 Tensile properties of CFs produced using 100% OL using different processing conditions. (a) Tensile strength; (b) tensile modulus.

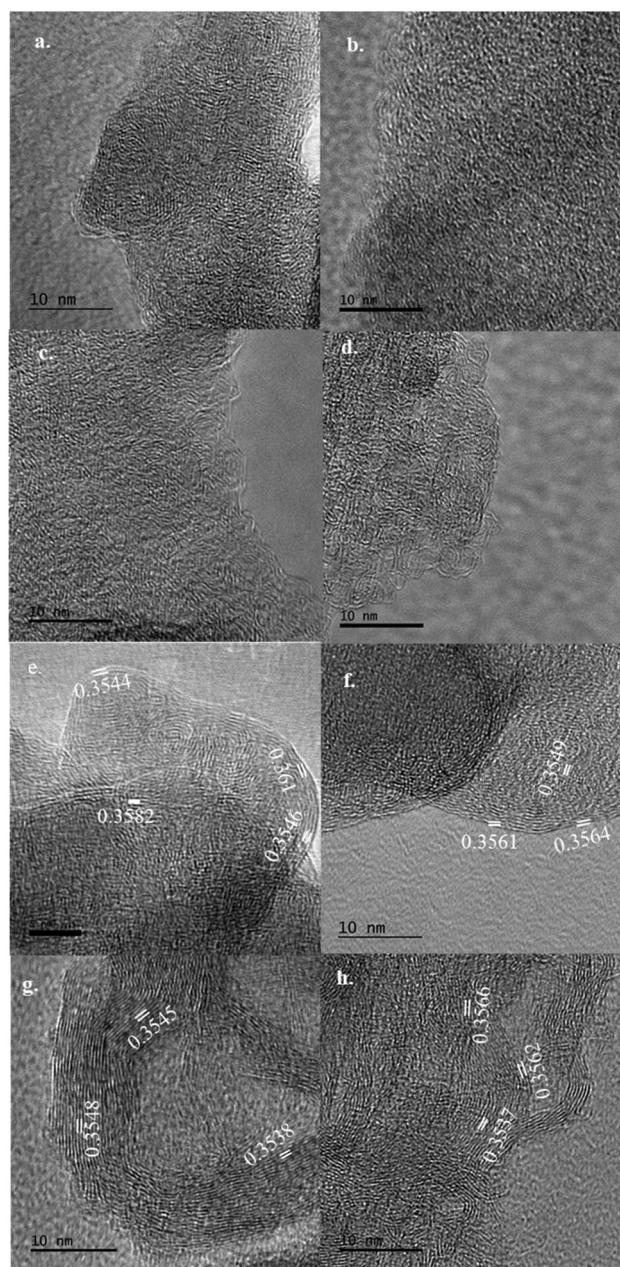**Fig. 4** TEM images of 100% OL-derived CFs. (a) NCF700; (b) NCF800; (c) NCF900; (d) NCF1000; (e) TCF700; (f) TCF800; (g) TCF900; (h) TCF1000.

tize even at temperatures above 2000 °C,[28] a turbostratic carbon structure was identified in TCF700 at a carbonization temperature of only 700 °C. In TCF700, disordered graphene layers are stacked to form an orderly, onion-like structure. In comparison, turbostratic carbons in TCF800 were less curved. With increasing temperature, longer-ranged ribbon-like graphene layers were observed in TCF900 and TCF1000.

3.3. Analysis of SF produced under different processing conditions

The changes in the microstructures of lignin are the results of chemical reactions that took place during the CF production process. The formation of turbostratic structure from lignin at such low temperatures without catalysts has been impossible previously, suggesting the thermomechanical controlling altered the ordinary chemical reactions and microstructural evolution from lignin. To support this statement, the chemical reactions and the microstructures were tracked by analyzing OL-based fibers at different stages under different processing conditions. This section discusses the effects of thermomechanical controlling on lignin stabilization.

3.3.1. Yields and tensile properties of SFs. TSF was obtained *via* a thermo-mechanically controlled stabilization, whereas NSF was prepared by a thermally controlled stabilization. Despite the heating profiles being identical for the two types of fibers, the yield of TSF was much lower than that of NSF (67% *vs.* 92%). Attributed to the increased mass loss and tension stretching, the average diameter of TSF was only 10 μm compared to 30 μm for NSF. On the other hand, the

Paper

tensile strength and modulus of TSF were 340.6 MPa and 29.1 GPa, respectively, compared to 154.8 MPa and 4.7 GPa for NSF.

3.3.2. HSQC-NMR results. HSQC-NMR spectroscopy was used to analyze the chemical structures of lignin, AF, TSF, and NSF. TSF and NSF stabilized up to 165 °C were analyzed here because the fibers stabilized at higher temperatures were only partly soluble in the solvent used for NMR analysis (fully stabilized fibers were analyzed in the rest of the article). Fig. 5 shows the NMR spectra of fibers at different C/H regions. The structure of AF was similar to that of lignin before fiber spinning, suggesting that melting spinning does not significantly alter lignin structure (Fig. 5a–d). In the oxygen-related regions (40–100 ppm/2.0–5.0 ppm of Fig. 5c, e, and g), the cross-peaks of original lignin structures, including β-O-4, β-5, and resinol β–β structures (the bond structures illustrated in Fig. 5g) reduced in both TSF and NSF compared to AF due to their bond cleavages during stabilization. The peaks at the aromatic region (100–160 ppm/5.0–8.0 ppm of Fig. 5a, c, and e) also decreased in both fibers, which is related to the condensation of individual aromatic rings to fused rings. Despite the similar changes after stabilization, NSF and TSF showed their distinc-

tively different molecular structures. Compared to NSF, there were significantly more bond cleavages for forming TSF. For example, the cross-peaks of C_α and C_β in β-O-4 can be observed in NSF, whereas they completely disappeared in TSF at the same temperature. While cross-peaks at the non-oxygen alkyl region (Fig. 5b, d, and f) increased after stabilization, significantly more peaks were observed in TSF than NSF. Stilbene and secoisolariciresinol structures observed in this region were much more abundant in TSF. Stilbene structure originates from β-5, β-1, or β-O-4, formed upon the bond cleavages followed by rearrangements.[33] Secoisolariciresinol structure is derived from β-O-4, formed *via* homolytic cleavages at its C_β–O followed by coupling two C_β carbon radicals and eliminating hydroxyl groups.[34] This structure can also be derived from resinol by cleaving its two symmetric C_α–O bonds. Both structures are linearly stretched and orientable. Several new cross-peaks were only presented in TSF at this region, corresponding to aliphatic structures with CH or CH_2 at C_α and CH, CH_2, or CH_3 at C_γ.[35] Apparently, TSF had a molecular structure with significantly improved linearly containing abundant alkyl linkages. Such a structure cannot be formed by heating lignin only.

Fig. 5 HSQC-NMR spectra of 100% OL-derived AF and SFs. (a & b) Lignin, (c & d) AF, (e & f) NSF stabilized up to 165 °C; (g & h) TSF stabilized up to 165 °C; (a, c, e, and g) are oxygen and aromatic-related regions. (b, d, f, and h) are non-oxygen aliphatic regions, and (i) the structures labeled in a–h.

lignin does not form graphene structures. I_D/I_G ratio in amorphous carbon materials is related to the abundance of benzene rings and side chain sp^2 carbons, increasing with amorphous sp^2 hybridized carbon content.[36] The I_D/I_G ratios at the cross-section and top views of the fiber were 0.85 and 0.82 for TSF, while they were 0.80 and 0.71 for NSF. The higher I_D/I_G ratios in TSF indicate that the fiber contains higher amorphous sp^2 carbons than NSF. D + D″ peak was also found in TSF in both directions with similar relative peak intensities. In comparison, the D + D″ peak was found only in the side-view spectra in NSF. This peak was previously reported in Raman spectra of highly oriented pyrolytic graphene, carbon nanotubes, or graphite paper[37,38] In graphite paper, the intensity of the D + D″ peak was much stronger in its top view of the graphite than in the side view due to its anisotropic structure.[38] Therefore, the Raman results suggest that NSF structure is anisotropic, whereas TSF structure is isotropic in different fiber directions.

3.3.6 Effects of thermo-mechanochemistry on lignin stabilization. Since identical heating profiles were used to produce TSF and NSF, the differences in their chemical structures and microstructures described above are due to the thermal and mechanical tension coupled controlling of spun fiber during its stabilization. The results described above suggest that applying strong mechanical force to stretch the spun fibers undergoing thermal treatment introduced the mechanochemistry of lignin in addition to ordinary thermochemistry. The coupled thermochemistry and mechanochemistry manipulated the conventional chemical reactions to transform lignin into a structure that is not easily formed by the thermochemistry of lignin alone under the same temperature conditions. Mechanochemistry refers to reactions induced by a mechanical force applied to molecules, which can cause a distinct transformation compared to thermochemical reactions caused by evaluating temperature.[39,40] In previous studies, mechanochemistry promoted bond scissions, pericyclic reactions, and isomerization in synthetic polymers.[41] The mechanochemistry of lignin is not well understood in literature, particularly when it is coupled with thermochemistry. A previous study reported that when lignin was ball milled, the friction force resulted in partial cleavages of C–O and C–C bonds between aromatic rings.[42] Since ball milling was usually conducted at room temperature, the effect of thermochemistry was minimal. In this work, mechanochemistry and thermochemistry can simultaneously play roles because strong tension was applied to spun fiber undergoing thermal treatment. If the spun fibers are stabilized without mechanical force or with an insignificant amount of force (which was the case for most of the previous lignin-based CFs), the chemical reactions of lignin would be driven solely by its thermochemistry. With increasing temperatures under an oxidative environment, heterogeneous side-chain functional groups of the aromatic rings are subjected to thermally induced bond cleavages, oxidation, repolymerization, and crosslinking in different fiber directions, leading to highly condensed and non-oriented structures containing an increased number of C=O. The characterization

results of TSF compared to NSF showed that coupling thermochemistry with mechanochemistry introduced thermo-mechanochemistry to promote bond cleavages in the irregular lignin structure because the molecules are activated by both thermal energy and mechanical energy. Previous studies showed that mechanochemistry-induced bond rupturing causes chain fragmentation to degrade polymer structure.[39] Thus, increasing interunit bond cleavages is supposed to reduce the mechanical strength of TSF. However, as described above, TSF had much higher tensile properties than NSF. Thus, the effect of thermo-mechanochemistry was more than deconstructing the heterogeneous polymer into smaller fragments. During the tension-applied stabilization, the partly cleaved lignin structures with reactive ends (i.e., radicals) are rearranged and repolymerized to form a new structure that is much stronger than the original lignin structure. The new structure is expected to consist of intra- or inter-molecular C–C or C–O linkages with high bond strengths aligned along the fiber axial direction because weaker bonds would not be able to survive the increasing temperature and the strong mechanical force simultaneously applied to the fibers. The weaker bonds of lignin (e.g., β-O-4) are likely eliminated and replaced by stronger bonds newly formed.

Mechanical stretching of the softening fiber also physically reduces fiber diameters during stabilization. The thinner fiber diameters of TSF can minimize heat transfer limitation during stabilization and promote uniform heat penetration toward the fiber core compared to NSF with thicker fiber diameters. Thus, the fiber surface and core structures are expected to be more uniform in TSF than in NSF. Although the extent of oxidation is supposed to be greater in TSF than in NSF, TSF has a lower carbonyl content and total oxygen content than NSF (elemental analysis results in Table S2†). The oxidation reactions in TSF likely promoted bond cleavages to release oxygenated volatile compounds and light gases rather than forming the end unit carbonyls. As indicated above, carbonyl and the residue hydroxyl groups were both lower in TSF than NSF. Thus, the aliphatic OHs were removed from lignin as volatile products rather than becoming C=O. Since hydroxyl groups are the major active sites for lignin to crosslink, removing them reduced lignin's tendency to crosslink, which was evident in TSF pyrolysis results. The yield of TSF was much lower than that of NSF, which supports that the increased bond scissions and rearrangements in TSF promote lightweight byproducts.

Plausible reactions of the major lignin linkages under thermo-mechanochemistry are given in Fig. 7. During conventional thermal oxidation of lignin, oxygen promotes the abstraction of hydrogen from alcohol groups. The remaining ether CH_2O radicals are stabilized to become terminal carbonyls. In comparison, the CH_2O radicals are removed as formaldehyde in the presence of tension due to an additional C–C bond dissociation promoted by the mechanochemistry effect. As described in literature,[39] external force can cause bond rotation, angle bending, and bond stretching to deform the original bond until the bond scission occurs. Deformed bonds
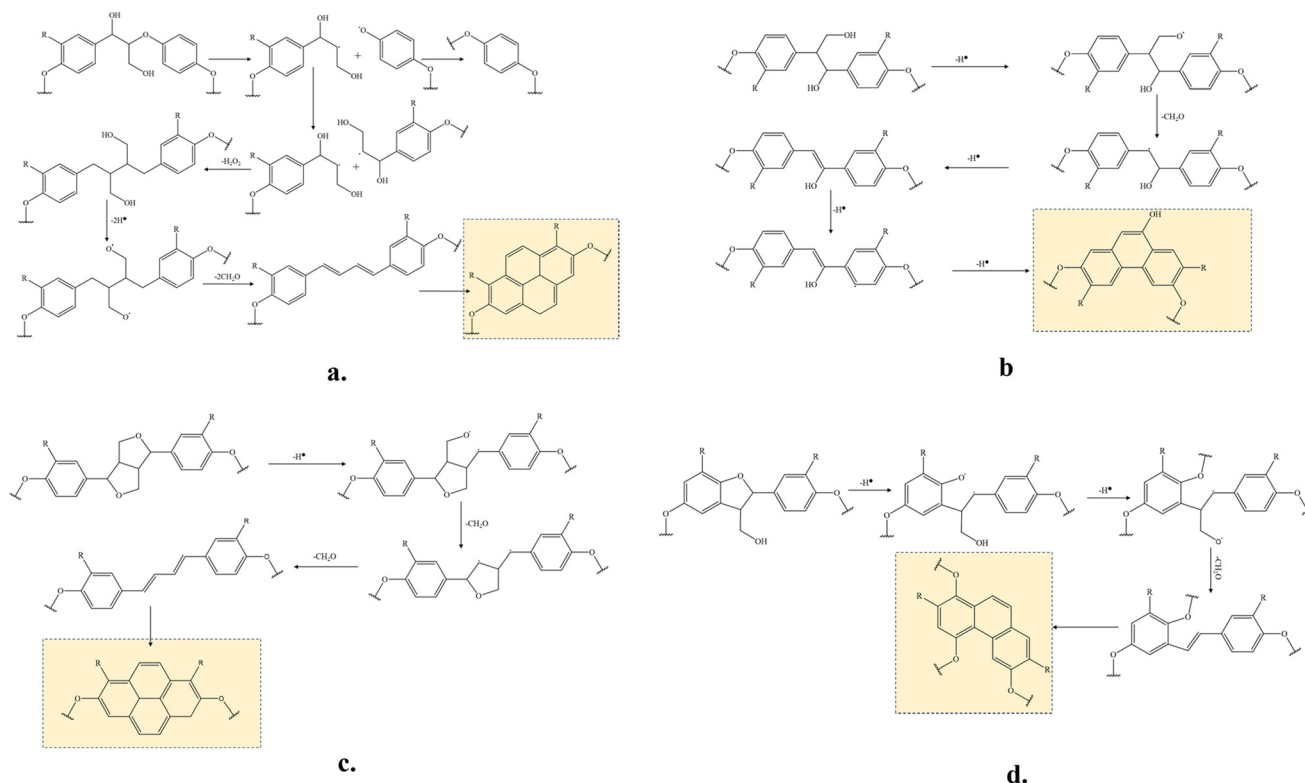
Fig. 7 Plausible reactions occurring during tension-applied stabilization of lignin spun fiber. (a) β-O-4; (b) β-1; (c) β–β; (d) β-5. The structures in the colored boxes are after carbonization.

have lower bond dissociation energies than free bonds. When tension is applied to stretch the bi-aromatic ring structures with interlinkages, the CH_2O radicals present at the branches of the aromatic interlinkages can depart from their original positions in the molecules by responding to the force. When tension force is strong enough, the homolytic carbon–carbon bond session between the CH_2O carbon and the adjacent alkyl carbon of the aromatic interlinkages will remove CH_2O entirely as a volatile byproduct. After CH_2O is removed, the remaining radical structures are stabilized to form linear aromatic structures with less branched interlinkages consisting of sp^2 carbons. In lignin under tension, the CH_2O radical can originate from hydrogen abstracted hydroxyls in β-O-4 or β-1 structures or ring-opening reactions of β–β or β-5 structures. Due to their orientability and sp^2 hybridized amorphous carbons, the newly formed molecular structures after the CH_2O removal can easily cyclize during continuous heat treatment by stabilization and carbonization. Beste[33] previously studied the oxidation of lignin model compounds by performing a molecular dynamic simulation using a reactive force field method. The removal of aliphatic OH as formaldehyde was among the possible reactions. However, cracking was the major reaction under the high simulation temperatures (>2000 K) because most of the oxidation products were gases and other lightweight molecules. Therefore, the probability of these reactions occurring in thermally treated lignin at real stabilization temperatures is expected to be low. As observed in NSF characterization, OH

groups were oxidized to become carbonyl groups after stabilization. Under tension, deconstructing and rearranging the irregular lignin structure to linearly stretched, orientable bi-aromatic ring structures and removing branched side chains with OHs to suppress random-directional crosslinking among molecules are expected to yield a structure with improved orientability and a higher content of graphitizable sp^2 carbons in TSF. Such a new structure is difficult to obtain by thermally treating lignin. The uniform structure with strong covalent bonds in TSF is expected to reduce the risk of mechanical failures within the fiber when an external force is applied to the fiber.

3.4 Analysis of CFs produced using different processing conditions

In this section, TSF and NSF were carbonized to different final temperatures using the same heating profiles but with different conditions for mechanical control. Different CFs were analyzed for their chemical and microstructural transformations during carbonization.

3.4.1 FTIR results. The FTIR spectra of different CFs are compared in Fig. 8a. For TCFs, the fibers produced using the carbonization temperatures from 500 to 1000 °C were analyzed to investigate how the molecular structure progresses during the carbonization with increasing temperature under tension. NCF800 and PCF800 were also analyzed to compare them with TCF800 to evaluate the tension effect. In the figure, the peaks
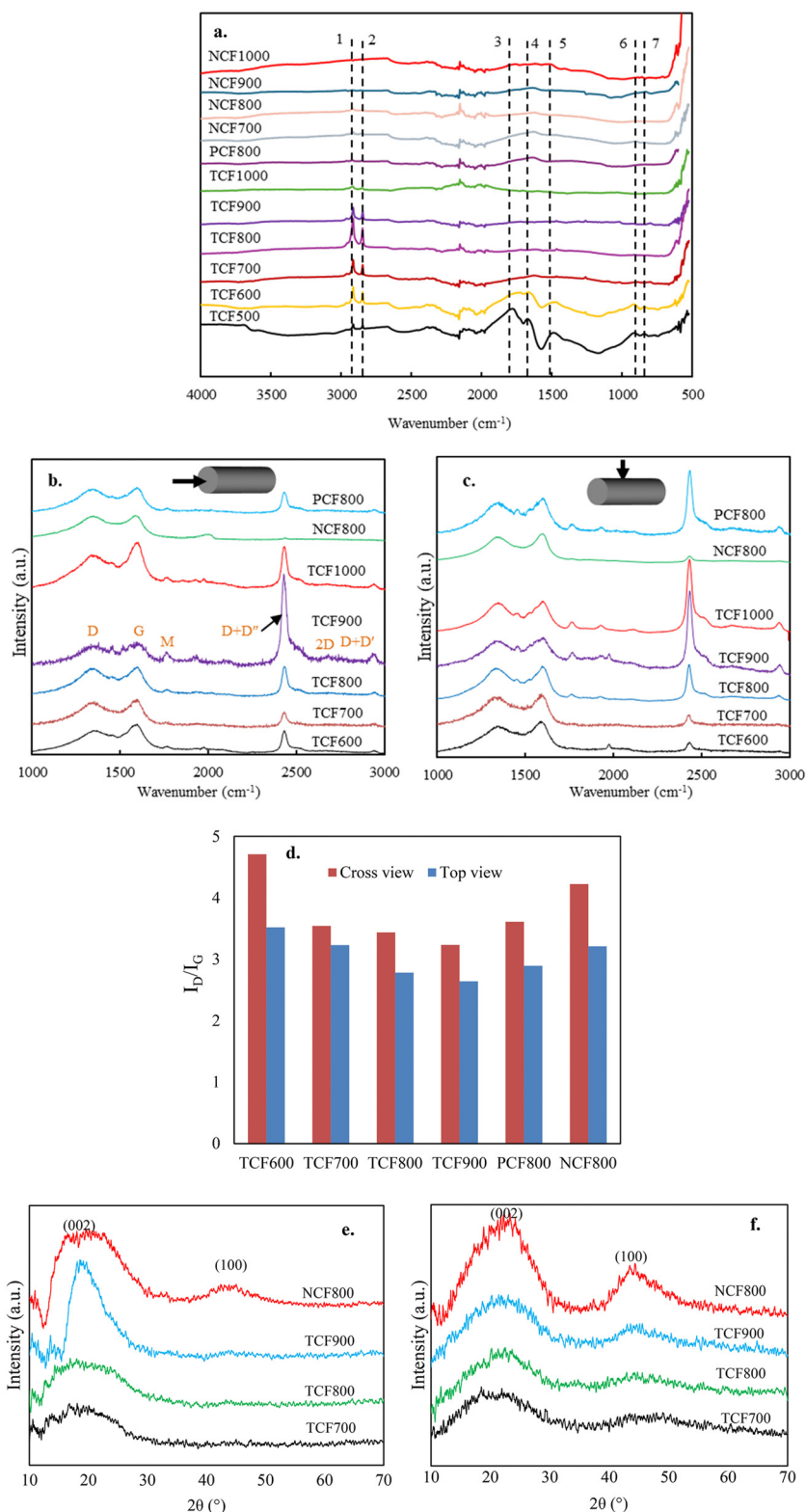
Fig. 8 Characterization of 100% OL-derived CFs. (a) FTIR spectra: 1 (2914 cm^{-1}) & 2 (2850 cm^{-1}) for alkyl C–H stretch, 3 (1760 cm^{-1}) & 4 (1650 cm^{-1}) for C=O, 5 (1500 cm^{-1}), 6 (913 cm^{-1}), and 7 (833 cm^{-1}) for aromatic ring vibration. (b–d) Raman spectra: (b) cross-section view spectra; (c) top view spectra; (d) I_D/I_G ratios of CFs in different fiber directions after Gaussian fitting; (e & f) XRD equatorial scans measured at (e) parallel and (f) perpendicular to the fiber axis.

associated with aromatic rings (peaks 5, 6, and 7), carbonyls (peaks 3 and 4), and hydroxyls vanished in TCF700 and other TCFs obtained using higher carbonization temperatures. These structures disappeared because higher carbonization temperature promotes deoxygenation and cyclization reactions to form fused benzene rings and nanocrystallites. Meanwhile, the intensity of the peaks representing the stretching vibrations of aliphatic C–H (peaks 1 and 2) increased in TCFs with increasing carbonization temperature up to 800 °C in TCF800. The new aliphatic bonds formed at high temperatures, suggesting that the nanocrystallites or fused rings were interconnected in TCFs through aliphatic linkages with high bond strengths. In their turbostratic carbon structures, the aliphatic linkages could present between graphene layers or at the edges of nanocrystallites. The aliphatic peaks started to decrease at TCF900 and TCF1000, likely because the linkages were either cleaved at higher temperatures or had undergone cyclic reactions. In comparison, the aliphatic peaks were either absent or weak in NCFs. The bands for aromatic ring vibration and carbonyls were visible even in NCF1000, suggesting a lower level of cyclization and a higher content of oxygen bonding in the CF when thermochemistry alone takes place. The aliphatic peaks nearly disappeared in PCF800 while they were the dominant peaks in TCF800. Recall that PCF was produced by carbonizing TSF in the absence of tension restriction. Thus, the stretched aliphatic linkages formed in TCFs are attributed to the tension force continuously applied to stretch TSF during its carbonization, and their presence increases the structural orientation of carbon fiber. Omitting tension stretching during carbonization seemed to severely hinder TSF from maintaining structural orientation when it was further carbonized.

3.4.2. XPS results. The carbon-containing bonds in different CFs were analyzed by X-ray photoelectron spectroscopy (XPS). The XPS spectra are shown in Fig. S6,† and the quantified results are summarized in Table 2 (analysis details in ESI†). The sum of –C–C and –C–H was 81.2% for TCF700. It became slightly lower for TCF800 and then increased for TCF900. On the other hand, the –O–C=O content decreased with increased temperatures to become negligible in TCF900. The –C=O content was lowest in TCF700 and increased at the fibers with higher carbonization temperatures. When compared with NCF800, TCF800 contained significantly fewer amounts of oxygen-bonded carbons. For example, the –O–C=O content was 22.3% in NCF800 whereas it was only 1.7% in TCF800. The XPS results correspond to the FTIR results of CFs, indicating that introducing thermo-mechanochemistry

can reduce oxygen-bonded carbons in CF. Oxygen-bonded carbons can hinder the growth of crystallites during carbonization.[43] Thus, the decreased oxygenated bonds are highly preferred for forming a graphene structure observed in TCFs.

3.4.3. Raman analysis results. The Raman spectra of CFs were measured at the cross-section and top views and the results are given in Fig. 8b–d. In Fig. 8b and c, the D and G peaks were broad due to the co-presence of graphene and disordered carbons, including amorphous carbons. Weak M and 2D peaks, representing graphene structures with ordered layers,[24] appeared in the TCFs as the carbonization temperature increased. D + D″ peak was observed in TCFs in both fiber directions at similar relative peak intensities. In comparison, D + D″ peaks were negligible in NCF800 in both Raman directions and much weaker in the cross-section view than in the top view of PCF800. Gaussian fitting was used to further analyze the D and G peaks (Fig. S7†). The I_D/I_G ratios of the CFs were calculated for two different directions in Fig. 8d (analysis details in ESI†). While I_D/I_G decreased in TCFs with increased carbonization temperature, the difference between the I_D/I_G at different fiber directions was the smallest for TCF700. Its Raman spectra distribution in two directions was similar, implying its isotropic structure. As the carbonization temperature increased, TCF800 and TCF900 became more anisotropic as the difference of their I_D/I_G in different fiber directions increased. As described above, the diameters of these fibers were larger than that of TCF700 due to stronger fiber shrinkage at higher carbonization temperatures. Thus, the increased anisotropic in these fibers is likely attributed to the fiber shrinkage and thicker fiber diameter. The increased anisotropic also corresponds to the decreased tensile properties in TCF800 and TCF900 compared to TCF700. For the CFs produced using the identical carbonization temperature, the I_D/I_G decreased in the order of NCF800 > PCF800 > TCF800 in both fiber directions. The decrease was much more obvious in the cross-section view of the fibers, suggesting that thermo-mechanochemistry introduced by tension force can enhance the graphitization and ordering at both the surfaces and inner fibers to promote uniform CF structures. The extent of anisotropic was greatest with NCF800, followed by PCF800, and least with TCF800, which is the opposite order of their tensile properties. This result confirms that the novel thermo-mechanochemistry introduced during stabilization and carbonization can greatly enhance the formation of graphene carbons and promote a CF structure with greater isotropic. PCF800 had a higher structural disorder and much lower tensile properties than TCF800, highlighting the importance of introducing thermo-mechanochemistry during carbonization in addition to stabilization.

3.4.4. XRD results. The XRD equatorial scans of CFs were performed parallel and perpendicular to the fiber axis. The results are shown in Fig. 8e and f. The first band was broad in all CFs due to the convolution of (002) and γ bands. The γ band, which occurs at 2θ below 20°, is usually attributed to aliphatic side chains attached to the edge of nanocrystallite.[44] In NCF800, (002) and (100) bands were observed in both scans.

Table 2 XPS results of 100% OL-based CFs

CFs	–C–C–/–C–H (%)	–C–O– (%)	–C=O (%)	–O–C=O (%)
TCF700	81.20	3.02	8.66	7.12
TCF800	71.58	8.67	18.30	1.45
TCF900	84.49	2.96	12.55	0.0
NCF800	57.40	9.15	11.18	22.27

Due to the random distribution of crystal plane orientations, two perpendicular crystal planes could be observed in both diffraction angles. In comparison, the (100) band was nearly absent in the parallel scans of TCFs. Although the appearance of both (100) and (002) bands in their perpendicular scans indicates that the crystals do not perfectly align, there was a preferred alignment in the fiber axial direction. Gaussian fitting of the XRD curves (Fig. S8†) was performed to calculate structural parameters (details in ESI†), and the results are shown in Table 3. In TCFs, the crystallite sizes (L_a and L_c) increased along with increased carbonization temperature due to the growth of graphite carbons. Due to aliphatic linkages between the layers, the interlayer spacings of TCFs were larger than that of the perfect graphene structure (0.335 nm). Compared to TCF800, NCF800 had larger-sized crystallites of larger interlaying spacing. However, these nanocrystals were randomly distributed without order, as shown in the TEM results. Crystalline ordering in TCFs, enabled by thermo-mechanochemistry, rather than crystallite size, is likely more important for delivering high tensile properties in the lignin-based CF.

3.4.5 SAXS analysis results. Small-angle X-ray scattering (SAXS) analysis was performed to analyze pore sizes in CFs (Fig. S9†). Table 4 lists the average pore diameters of different CFs calculated based on SAXS results (details in ESI†). Along with other factors, fiber pores can significantly affect the mechanical properties of CFs. In addition to creating physical defects, the fiber pores hinder the growth of crystallites perpendicular to the graphene planes.[45] Large pores have stronger detrimental effects on mechanical properties than smaller pores since they can more easily introduce crack propagations.[46] The pore size was much smaller for TCF800 than NCF800 (1.991 nm compared to 2.5 nm), indicating thermo-mechanochemistry also inhibited pore growth in CFs. Recall that the thermo-mechanochemistry introduced during lignin stabilization under tension promoted the removal of weak bonds in TSF and suppressed new carbonyl formation. If the

weak bonds were not removed during stabilization, they would be cleaved during carbonization to increase gas byproducts, promoting pores in the solidified CFs. Carbonyls present in SFs are the source of CO_2 and CO during carbonization, which can increase fiber pores. Accordingly, removing the weak bonds and limiting carbonyl formation during stabilization is expected to reduce gas formation during the carbonization and, thus, inhibit pore growth in TCFs. It shows that the pore sizes of TCFs are strongly correlated with their carbonization temperatures, increasing with increasing temperature. The pore size was only 0.815 nm for TCF700, much smaller than that for TCF800 and TCF900. The turbostratic structure with interlocked disordered carbons, isotropic structure, and small pores in TCF700 are expected to prevent crack propagation of the pores beyond the limit for catastrophic failure from the extensive crystalline walls, leading to high tensile properties. Recall that the tensile properties of TCFs were the highest with TCF700 and decreased with increasing carbonization temperature. Although the graphitization degree increased in the TCFs obtained with higher carbonization temperatures, they also had higher fiber diameters, increased anisotropic, and larger pore sizes. Crack propagation-induced mechanical failure is expected to be more pronounced under such conditions, resulting in decreased tensile properties in these fibers.

3.4.6. The role of thermo-mechanochemistry in forming CF. During stabilization, thermo-mechanochemistry enhanced the disassembly of the irregular lignin structure to remove weak interunit bonds and branched side chains and controlled the rearrangement reactions to form a linearly stretched, orientable structure. The new structure contained fewer oxygen-related bonds and more sp^2 hybridized carbons, which is also more isotopic than the structure generated by the thermo-chemistry of lignin. Our results show that such a structure is readily graphitized using unprecedently low carbonization temperatures and produces fewer fiber pores during carbonization.

While the thermo-mechanochemistry introduced during stabilization could manipulate and modify ordinary thermo-chemical reactions of lignin to transform the irregular molecular structure into a much-desired structure in TSF, introducing thermo-mechanochemistry during carbonization was important in ensuring the evolution of ordered microstructures from TSF. During carbonization, a strong tendency for fiber shrinkage along the fiber direction was only observed with TSF. When the stabilization of lignin occurs in the absence of thermo-mechanochemistry, various functional groups could freely interact in random directions of the fiber to form highly crosslinked and non-oriented structures. Thus, carbonizing NSF did not show noticeable fiber shrinkage. TSF exhibited the shrinking tendency, suggesting the oriented molecular structure of the stabilized fiber stretched along the fiber direction retains high chemical reactivity. TSF was less crosslinked and condensed than NSF, implying that the strong force applied to the fiber mechanically restricted the freedom of the molecular structure to prevent the intermolecular bonds from developing crosslinking in undesired fiber directions. If

Table 3 Structural parameters of 100% OL-based CFs based on XRD results

	TCF700	TCF800	TCF900	NCF800
d_{002} (nm)	0.3675	0.3572	0.3516	0.3697
L_c (nm)	0.6155	0.8047	1.1003	0.9647
L_a (nm)	1.0725	1.2029	1.3434	1.9109

Table 4 Porosity analysis of 100% OL-based CFs based on SAXS results

	b^a	R^b
TCF700	0.2577	0.815
TCF800	0.6296	1.991
TCF900	0.6736	2.130
NCF800	0.7905	2.500

^{a} b (nm) is the Debye autocorrelation length of the pores. ^{b} R (nm) is the radius of the pore.

TSF is carbonized in the absence or with insufficient mechanical restrictions, the functional groups remaining in the no-longer restricted structure could freely react in different directions, causing the fiber to shrink. Allowing the fiber shrinkage during carbonization will lead to a microstructure with increased structural disorder and anisotropic, eventually lowering the mechanical properties in CF. In comparison, applying sufficient high force to restrict the fiber will ensure the oriented structure of TSF crosslinks only at the desired fiber direction as it carbonizes, which was critical in forming ordered microstructures and graphene carbons in TCF.

Until this study, it has been considered that the non-oriented amorphous carbons and low-tensile properties of CFs are unavoidable with lignin precursors. However, our results show that it is possible to overcome this challenging problem using a facile approach by controlling heat and mechanical force applied to lignin-derived fibers. Properly integrating thermal heating and mechanical stretching can introduce a novel thermo-mechanochemistry, which can manipulate ordinary chemical reactions to modify the molecular structure and control microstructural evolution, transforming lignin into an oriented structure with graphitized carbons. Our results suggest that the high tensile properties in lignin-based CF obtained in this work are due to the combined effects of structural ordering, isotropic structure, turbostratic carbons, and smaller pore sizes. TCF700 produced using the extremely low carbonization temperature had the highest tensile properties because the fiber could meet all these conditions, contributed by the newly introduced thermo-mechanochemistry. Unlike conventionally produced CFs, the tensile properties decreased at the TCFs produced at higher carbonization temperatures because the negative impacts caused by the increased anisotropic structure and larger pore size at these fibers were more prominent than the positive impact of the increased graphitization.

In this work, TSFs produced at low carbonization temperatures had both high tensile strength and modulus. Even for PAN-based CFs, carbonization temperatures above 1000 °C are usually required to obtain comparable tensile properties. PAN-based and lignin-based CF differ in their completely different molecular structures and reaction mechanisms for forming CF. PAN is a linear-chain polymer without ring structures. Thus, PAN must form individual benzene rings from scratch through extensive cyclization during stabilization and carbonization. In comparison, lignin intrinsically owns benzene rings in their basic units. By introducing thermo-mechanochemistry during stabilization, benzene rings are interconnected by stable aliphatic bonds to form an oriented structure susceptible to graphitization. Introducing thermo-mechanochemistry during the subsequent carbonization further promoted graphene structure by ensuring orientation and preventing undesired crosslinking. Since the benzene ring structure is already present in TSF, its graphitization can occur at a much lower temperature than the temperature required for PAN-based CFs, as confirmed by the TEM results above. Turbostratic structure and polyaromatic ring clusters in TCFs are connected *via*
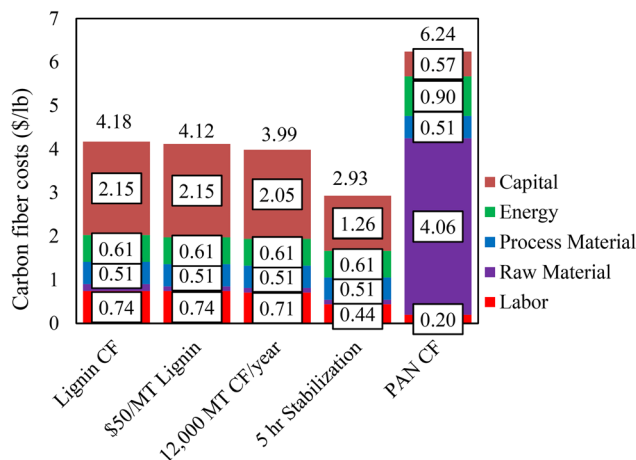

Fig. 9 Comparison of current and projected production costs of lignin-based CF based on this work to literature-estimated PAN-based CF production cost (12).

strong aliphatic linkages, increasing both the strength and rigidity of the material.

3.5. Techno-economic analysis of lignin-based CF

The above results show that CFs with mechanical properties exceeding the DOE targets could be produced using lignin alone based on the melt-spinning method. A preliminary techno-economic analysis (TEA) was conducted to determine the cost of melt-spun lignin-based CF. The cost estimation was based on a 10 000 MT per year facility, with a lignin purchase price of $110 per MT and a 10-hour stabilization time as the base case (equivalent to the case for the 80%/20% OL/KL-based CF in this work). In Fig. 9, our current and projected lignin-based CF costs are compared to a literature-estimated cost of PAN-based CF.[12] The results showed that the current production cost of lignin-based CF is estimated at $4.17 per lb, which is lower than that of the DOE automobile-grade CF. The impacts of techno-economic improvements on lignin-based cost projections were also studied. The cost can be reduced by lowering the lignin purchase price and increasing the plant capacity. Decreasing the lignin price to $50 per MT lowers the CF cost by $0.05 per lb to $4.12 per lb, and increasing the plant capacity by 20% decreases the cost by $0.19 per lb to $3.98 per lb. On the other hand, decreasing the stabilization time from 10 hours to 5 hours decreased costs by $1.25 per lb to $2.92 per lb. This work shows that the stabilization time is directly related to the precursor T_g. Extended stabilization hours were required in this work due to the low T_gs of the lignin precursors. We expect a substantial reduction in stabilization time when high T_g lignins are used.

4. Conclusions

This work demonstrated the production of low-cost high-quality CFs using lignin alone without chemical treatment or

additives. The property advancement is due to the introduction of thermo-mechanochemistry of lignin that is discovered in this work. This novel chemistry can be introduced by properly integrating thermal heating and mechanical stretching. The integration can transform lignin into oriented and graphene carbons by manipulating its chemical reactions and controlling the microstructure evolution. The proof-of-concept CFs demonstrated in the laboratory have smaller fiber diameters than commercial CFs, which are 5–8 μm. However, our results suggest that CF with higher tensile properties at industrial-relevant fiber diameters is expected when the fiber fabrication system with precision control is employed to fine-tune the heating and tension profiles. The discovery of the thermomechanochemistry of lignin and the improved understanding of lignin-based CFs reported in this work provide critical knowledge for developing a facile and green approach to enable high-quality CFs from broader lignin. Low-cost lignin-based CFs will simultaneously address the demands for low-cost green CFs in industries and the biorefinery bottleneck on lignin valorization.

Author contributions

Conceptualization: X.B. Methodology: Y.L., M.R., A.M, W.Q., A.A., H.Z, Investigation: Y.L. M.R., W.Q. Writing – original draft: Y.L., M. R., A.A. writing – review & editing: X.B., X.W., M.M.W. funding acquisition: X.B. Supervision: X.B.

Conflicts of interest

X. B, Y. L, and M. R along with Iowa State University Research Foundation have filed a US patent application no 18/495185.

Acknowledgements

References

1 J. Ragauskas, G. T. Beckham, M. J. Biddy, R. Chandra, F. Chen, M. F. Davis, B. H. Davison, R. A. Dixon, P. Gilna, M. Keller, P. Langan, A. K. Naskar, J. N. Saddler, T. J. Tschaplinski, G. A. Tuskan and C. E. Wyman, Lignin valorization: Improving lignin processing in the biorefinery, *Science*, 2014, **344**, 6185.

2 S. Sethupathy, G. M. Morales, L. Gao, H. Wang, B. Yang, J. Jiang, J. Sun and D. Zhu, Lignin valorization: Status, challenges and opportunities, *Bioresour. Technol.*, 2022, **347**, 126696.

3 D. S. Bajwa, G. Pourhashem, A. H. Ullah and S. G. Bajwa, A concise review of current lignin production, applications, products and their environment impact, *Ind. Crops Prod.*, 2019, **139**, 111526.

4 E. Frank, L. M. Steudle, D. Ingildeev, J. M. Spörl and M. R. Buchmeiser, Carbon fibers: Precursor systems, processing, structure, and properties, *Angew. Chem., Int. Ed.*, 2014, **53**, 5262–5298.

5 S. Wang, J. Bai, M. T. Innocent, Q. Wang, H. Xiang, J. Tang and M. Zhu, Lignin-based carbon fibers: Formation, modification and potential applications, *Green Energy Environ.*, 2021, **7**, 578–605.

6 W. Qu, J. Yang, X. Sun, X. Bai, H. Jin and M. Zhang, Towards producing high-quality lignin-based carbon fibers: A review of crucial factors affecting lignin properties and conversion techniques, *Int. J. Biol. Macromol.*, 2021, **189**, 768–784.

7 W. J. Sagues, A. Jain, D. Brown, S. Aggarwal, A. Suarez, M. Kollman, S. Park and D. S. Argyropoulos, Are lignin-derived carbon fibers graphitic enough?, *Green Chem.*, 2019, **21**, 4253–4265.

8 M. Pervaiz, S. Panthapulakkal, B. K. C. M. Sain and J. Tjong, Emerging Trends in Automotive Lightweighting through Novel Composite Materials, *Mater. Sci. Appl.*, 2016, **07**, 26–38.

9 Mordor Intelligence™ Industry Reports. Automotive carbon fiber market-growth, trends, Covid-19 impact, and forecast (2023–2028), **https://www.mordorintelligence.com/industry-reports/automotive-carbon-fiber-composites-market#:~:text=MarketOverview**, the forecast period 2022–2027, (accessed 2023 Oct 5).

10 Global Market Insights, Carbon Fibre Composites Market Size, Share and Industry Analysis Report by End-Use (Aerospace, Automotive, Wind Turbines, Sport & Leisure, Civil Engineering, Marine), and Matrix Material (Polymer [Thermosetting, Thermoplastics], Carbon, Ceramic, Metal. Report ID: GMI2180 07/2022., **https://www.gminsights.com/industry-analysis/carbon-fibre-composites-market?gclid=CjwKCAjwq-WgBhBMEiwAzKSH6H6eBA4G-e9ctCOk2zLuCYrqhK45mwJjsvJ__N-qGfUIMIosUEwwTBoCYGMQAvD_BwE**, (accessed 2023 Oct 5).

11 D. A. Baker and T. G. Rials, Recent advances in low-cost carbon fiber manufacture from lignin, *J. Appl. Polym. Sci.*, 2013, **130**, 713–728.

12 T. Ellringmann, C. Wilms, M. Warnecke, G. Seide and T. Gries, Carbon fiber production costing: A modular approach, *Text. Res. J.*, 2016, **86**, 178–190.

13 J. Mikkilä, M. Trogen, K. A. Y. Koivu, J. Kontro, J. Kuuskeri, R. Maltari, Z. Dekere, M. Kemell, M. R. Mäkelä, P. A. Nousiainen, M. Hummel, J. Sipilä and K. Hildén, Fungal Treatment Modifies Kraft Lignin for Lignin- And Cellulose-Based Carbon Fiber Precursors, *ACS Omega*, 2020, **5**, 6130–6140.

14 J. Jin, J. Ding, A. Klett, M. C. Thies and A. A. Ogale, Carbon Fibers Derived from Fractionated-Solvated Lignin Precursors for Enhanced Mechanical Performance, *ACS Sustainable Chem. Eng.*, 2018, **6**, 14135–14142.

15 K. H. K. Chan, S. Y. Wong, X. Li, Y. Z. Zhang, P. C. Lim, C. T. Lim, M. Kotaki and C. B. He, Effect of molecular

orientation on mechanical property of single electrospun fiber of poly[(R)-3-hydroxybutyrate-co-(R)-3-hydroxyvalerate], *J. Phys. Chem. B*, 2009, **113**, 13179–13185.

16 P. Azadi, O. R. Inderwildi, R. Farnood and D. A. King, Liquid fuels, hydrogen and chemicals from lignin: A critical review, *Renewable Sustainable Energy Rev.*, 2013, **21**, 506–523.

17 Q. Li, M. Li, H. S. Lin, C. Hu, P. Truong, T. Zhang, H. J. Sue, Y. Pu, A. J. Ragauskas and J. S. Yuan, Non-solvent fractionation of lignin enhances carbon fiber performance, *ChemSusChem*, 2019, **12**, 3249–3256.

18 W. Qu and X. Bai, Thermal treatment of pyrolytic lignin and polyethylene terephthalate toward carbon fiber production, *J. Appl. Polym. Sci.*, 2020, **137**, 1–10.

19 J. Jin and A. A. Ogale, Carbon fibers derived from wet-spinning of equi-component lignin/polyacrylonitrile blends, *J. Appl. Polym. Sci.*, 2018, **135**, 1–9.

20 A. Bengtsson, J. Bengtsson, M. Sedin and E. Sjöholm, Carbon Fibers from Lignin-Cellulose Precursors: Effect of Stabilization Conditions, *ACS Sustainable Chem. Eng.*, 2019, **7**, 8440–8448.

21 M. Culebras, A. Beaucamp, Y. Wang, M. M. Clauss, E. Frank and M. N. Collins, Biobased Structurally Compatible Polymer Blends Based on Lignin and Thermoplastic Elastomer Polyurethane as Carbon Fiber Precursors, *ACS Sustainable Chem. Eng.*, 2018, **6**, 8816–8825.

22 H. C. Liu, J. Luo, H. Chang, A. A. B. Davijani, P. H. Wang and S. Kumar, Polyacrylonitrile sheath and polyacrylonitrile/lignin core bi-component carbon fiber, *Carbon*, 2019, **149**, 165–172.

23 W. Qu, Y. Huang, Y. Luo, S. Kalluru, E. Cochran, M. Forrester and X. Bai, Controlled Radical Polymerization of Crude Lignin Bio-oil Containing Multihydroxyl Molecules for Methacrylate Polymers and the Potential Applications, *ACS Sustainable Chem. Eng.*, 2019, **7**, 9050–9060.

24 Y. Luo, W. Qu, E. Cochran and X. Bai, Enabling high-quality carbon fiber through transforming lignin into an orientable and melt-spinnable polymer, *J. Cleaner Prod.*, 2021, **307**, 127252.

25 D. Choi, H. S. Kil and S. Lee, Fabrication of low-cost carbon fibers using economical precursors and advanced processing technologies, *Carbon*, 2019, **142**, 610–649.

26 J. L. Braun, K. M. Holtman and J. F. Kadla, Lignin-based carbon fibers: Oxidative thermostabilization of kraft lignin, *Carbon*, 2005, **43**, 385–394.

27 M. Zhang and A. A. Ogale, Carbon fibers from dry-spinning of acetylated softwood kraft lignin, *Carbon*, 2014, **69**, 626–629.

28 F. Torres-Canas, A. Bentaleb, M. Föllmer, J. Roman, W. Neri, I. Ly, A. Derré and P. Poulin, Improved structure and highly conductive lignin-carbon fibers through graphene oxide liquid crystal, *Carbon*, 2020, **163**, 120–127.

29 Q. Li, C. Hu, M. Li, P. Truong, J. Li, H. S. Lin, M. T. Naik, S. Xiang, B. E. Jackson, W. Kuo, W. Wu, Y. Pu,

A. J. Ragauskas and J. S. Yuan, Enhancing the multi-functional properties of renewable lignin carbon fibersviadefining the structure-property relationship using different biomass feedstocks, *Green Chem.*, 2021, **23**, 3725–3739.

30 S. Zhou, Y. Xue, A. Sharma and X. Bai, Lignin Valorization through Thermochemical Conversion: Comparison of Hardwood, Softwood and Herbaceous Lignin, *ACS Sustainable Chem. Eng.*, 2016, **4**, 6608–6617.

31 J. J. Adams, F. Nicola, F. Ray, G. Amit, A. Charlie, N. Amit and K. Logan, Consortium for Production of Affordable Carbon Fibers in the United States, 2021, DOI: **10.2172/1829480**.

32 D. J. Johnson, I. Tomizuka and O. Watanabe, The fine structure of lignin-based carbon fibres, *Carbon*, 1975, **13**, 321–325.

33 A. Beste, ReaxFF study of the oxidation of softwood lignin in view of carbon fiber production, *Energy Fuels*, 2014, **28**, 7007–7013.

34 M. H. Lahtinen, J. Mikkilä, K. S. Mikkonen and I. Kilpeläinen, Kraft Process - Formation of Secoisolariciresinol Structures and Incorporation of Fatty Acids in Kraft Lignin, *J. Agric. Food Chem.*, 2021, **69**, 5955–5965.

35 C. Mattsson, S. I. Andersson, T. Belkheiri, L. E. Åmand, L. Olausson, L. Vamling and H. Theliander, Using 2D NMR to characterize the structure of the low and high molecular weight fractions of bio-oil obtained from LignoBoost™ kraft lignin depolymerized in subcritical water, *Biomass Bioenergy*, 2016, **95**, 364–377.

36 X. Li, J. Hayashi and C. Z. Li, FT-Raman spectroscopic study of the evolution of char structure during the pyrolysis of a Victorian brown coal, *Fuel*, 2006, **85**, 1700–1707.

37 T. Shimada, T. Sugai, C. Fantini, M. Souza, L. G. Cançado, A. Jorio, M. A. Pimenta, R. Saito, A. Gruneis, G. Dresselhaus, M. S. Dresselhaus, Y. Ohno, T. Mizutani and H. Shinohara, Origin of the 2450 cm-1 Raman bands in HOPG, single-wall and double-wall carbon nanotubes, *Carbon*, 2005, **43**, 1049–1054.

38 R. Wang, H. Zobeiri, H. Lin, W. Qu, X. Bai, C. Deng and X. Wang, Anisotropic thermal conductivities and structure in lignin-based microscale carbon fibers, *Carbon*, 2019, **147**, 58–69.

39 G. D. Bo, Mechanochemistry of the mechanical bond, *Chem. Sci.*, 2017, **9**(1), 15–21.

40 J. Li, C. Nagamani and J. S. Moore, Polymer Mechanochemistry: From Destructive to Productive, *Acc. Chem. Res.*, 2015, **48**, 2181–2190.

41 E. Izak-Nau, D. Campagna, C. Baumann and R. Göstl, Polymer mechanochemistry-enabled pericyclic reactions, *Polym. Chem.*, 2020, **11**, 2274–2299.

42 S. Dabral, H. Wotruba, J. G. Hernández and C. Bolm, Mechanochemical Oxidation and Cleavage of Lignin β-O-4 Model Compounds and Lignin, *ACS Sustainable Chem. Eng.*, 2018, **6**, 3242–3254.

43 J. D. Kim, J. S. Roh and M. S. Kim, Effect of carbonization temperature on crystalline structure and properties of iso-

tropic pitch-based carbon fiber, *Carbon Lett.*, 2017, **21**, 51–60.

44 O. O. Sonibare, T. Haeger and S. F. Foley, Structural characterization of Nigerian coals by X-ray diffraction, Raman and FTIR spectroscopy, *Energy*, 2010, **35**, 5347–5353.

45 W. Dun, L. Guijian, S. Ruoyu and F. Xiang, Investigation of structural characteristics of thermally metamorphosed coal by FTIR spectroscopy and X-ray diffraction, *Energy Fuels*, 2013, **27**, 5823–5830.

46 A. R. Chambers, J. S. Earl, C. A. Squires and M. A. Suhot, The effect of voids on the flexural fatigue performance of unidirectional carbon fibre composites developed for wind turbine applications, *Int. J. Fatigue*, 2006, **28**, 1389–1398.

47 S. Kubo and J. F. Kadla, Lignin-based carbon fibers: Effect of synthetic polymer blending on fiber properties, *J. Polym. Environ.*, 2005, **13**, 97–105.

48 Y. Nordström, I. Norberg, E. Sjöholm and R. Drougge, A new softening agent for melt spinning of softwood kraft lignin, *J. Appl. Polym. Sci.*, 2013, **129**, 1274–1279.

49 D. A. Baker, F. S. Baker and N. C. Gallego, Thermal Engineering of Lignin for Low-cost Production of Carbon Fiber, in The Fiber Society 2009 Fall Confer-ence, University of Georgia, Athens, GA, USA, 2009, **https://www.thefibersociety.org/Portals/0/PastConferences/2009_Fall_Abstracts.pdf**, (accessed 2023 Oct 5).

50 L. Salmén, E. Bergnor, A. M. Olsson, M. Åkerström and A. Uhlin, Extrusion of Softwood Kraft Lignins as Precursors for Carbon Fibres, *BioResources*, 2015, **10**, 7544–7554.

51 N. Meek, D. Penumadu, O. Hosseinaei, D. Harper, S. Young and T. Rials, Synthesis and characterization of lignin carbon fiber and composites, *Compos. Sci. Technol.*, 2016, **137**, 60–68.

52 O. Hosseinaei, D. P. Harper, J. J. Bozell and T. G. Rials, Improving processing and performance of pure lignin carbon fibers through hardwood and herbaceous lignin blends, *Int. J. Mol. Sci.*, 2017, **18**(7), 1410.

53 K. Sudo and K. Shimizu, A new carbon fiber from lignin, *J. Appl. Polym. Sci.*, 1992, **44**, 127–134.

54 K. Sudo, K. Shimizu, N. Nakashima and A. Yokoyama, A new modification method of exploded lignin for the prepa-

ration of a carbon fiber precursor, *J. Appl. Polym. Sci.*, 1993, **48**, 1485–1491.

55 W. Qu, Y. Xue, Y. Gao, M. Rover and X. Bai, Repolymerization of pyrolytic lignin for producing carbon fiber with improved properties, *Biomass Bioenergy*, 2016, **95**, 19–26.

56 L. M. Steudle, E. Frank, A. Ota, U. Hageroth, S. Henzler, W. Schuler, W. Neupert and M. R. Buchmeiser, Carbon Fibers Prepared from Melt Spun Peracylated Softwood Lignin: an Integrated Approach, *Macromol. Mater. Eng.*, 2017, **302**, 1–11.

57 W. Qu, J. Liu, Y. Xue, X. Wang and X. Bai, Potential of producing carbon fiber from biorefinery corn stover lignin with high ash content, *J. Appl. Polym. Sci.*, 2018, **135**, 1–11.

58 D. Kang, Y. Lee, K. H. Park, J. S. Bae, S. M. Jo and S. S. Kim, Carbon Fibers Derived from Oleic Acid-Functionalized Lignin via Thermostabilization Accelerated by UV Irradiation, *ACS Sustainable Chem. Eng.*, 2021, **9**, 5204–5216.

59 J. F. Kadla, S. Kubo, R. A. Venditti, R. D. Gilbert, A. L. Compere and W. Griffith, Lignin-based carbon fibers for composite fiber applications, *Carbon*, 2002, **40**, 2913–2920.

60 W. Qin and J. F. Kadla, Effect of organoclay reinforcement on lignin-based carbon fibers, *Ind. Eng. Chem. Res.*, 2011, **50**, 12548–12555.

61 A. Bengtsson, P. Hecht, J. Sommertune, M. Ek, M. Sedin and E. Sjöholm, Carbon Fibers from Lignin-Cellulose Precursors: Effect of Carbonization Conditions, *ACS Sustainable Chem. Eng.*, 2020, **8**, 6826–6833.

62 P. J. Bissett and C. W. Herriott, Lignin/polyacrylonitrile-containing dopes, fibers and production methods, *US Patent: US Patent*; US 2012/0003471A1, 2010.

63 H. C. Liu, A. T. Chien, B. A. Newcomb, Y. Liu and S. Kumar, Processing, Structure, and Properties of Lignin- and CNT-Incorporated Polyacrylonitrile-Based Carbon Fibers, *ACS Sustainable Chem. Eng.*, 2015, **3**, 1943–1954.

64 Q. Ouyang, K. Xia, D. Liu, X. Jiang, H. Ma and Y. Chen, Fabrication of partially biobased carbon fibers from novel lignosulfonate–acrylonitrile copolymers, *J. Mater. Sci.*, 2017, **52**, 7439–7451.